WORLD CONFERENCE ON TIMBER ENGINEERING 2025
BRISBANE, AUSTRALIA
Advancing Timber for the Future Built Environment

STRUCTURAL PERFORMANCE OF TIMBER FRAMES WITH CONCRETE BEAM-COLUMN JOINT EXPOSED TO CYCLIC LOADING

Tomoyuki Hayashi[1] , Daiki Hinata[2] , Shinji Takatani[3], Keisuke Yamaguchi[4], Jun Kubota[5]

ABSTRACT: In recent years, as environmental considerations have continued to grow, attention has turned to reducing CO_2 emissions through the carbon fixation effect of wood. Traditionally, timber frame connections have been designed as pin or semi-rigid connections in structural design due to the wood's weak properties perpendicular to the grain. This has made it challenging to implement timber frame structures in high seismic regions. However, more effective moment transmission at connections may allow for flexible floor plans and rational structural designs with fewer lateral resisting components. In this study, we developed a new beam-column joint consisting of reinforced concrete (RC) and a glued-in rod (GIR) with high stiffness. We evaluated the structural properties by conducting full-scale partial frame tests. The results showed that the timber frames exhibited high stiffness, strength, and excellent ductility. Additionally, the theoretical equation adopted for the joint accurately estimated both the stiffness and yield strength.

KEYWORDS: *timber frames, beam-column joint, reinforced concrete, glued-in rod*

1 – INTRODUCTION

Efforts towards environmental conservation have intensified, necessitating the construction industry to advance towards a decarbonized society. In this context, the carbon sequestration potential of wood has garnered attention as a viable strategy for reducing carbon footprints. Recently, there has been a surge in projects prioritizing environmental sustainability through the utilization of mass timber, including cross-laminated timber (CLT) panels and glued laminated timber (glulam) beams. Typically, the ends of beams and columns have been designed as pin or semi-rigid connections, resulting in inefficient bending moment transfer due to the limited stiffness of wood in the perpendicular direction to the grain. Rigid beam-column joints must be implemented for a more rational structural design. A glued-in rod (GIR) connection, wherein steel rods are inserted into drilled holes within timber members and cured with epoxy resin, presents a promising solution that offers greater stiffness and strength compared to traditional timber connections. Although several moment connections utilizing GIR have been proposed and investigated[1][2][3], there remains a pressing need for improved force transmission efficiency. In this study, we have developed an innovative beam-column joint integrating reinforced concrete (RC) and GIR to enhance stiffness. We propose the beam-column joint shown in Figure 1, which incorporates reinforced concrete at the intersection of the column and beam, featuring design elements that address the vulnerabilities associated with traditional moment-resisting joints, particularly when the embedding is perpendicular to the grain. In this joint,

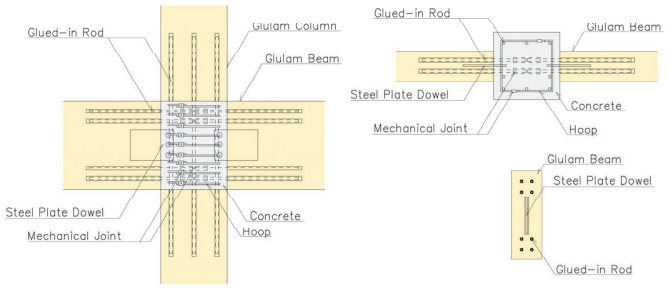

Figure 1. Beam-column joint detail.

[1] Tomoyuki Hayashi, Architectural Design Division, Kajima Corporation, Tokyo, Japan, hayatomo@kajima.com

[2] Daiki Hinata, Kajima Technical Research Institute, Kajima Corporation, Tokyo, Japan, hinata@kajima.com

[3] Shinji Takatani, Architectural Design Division, Kajima Corporation, Tokyo, Japan, takatani@kajima.com

[4] Keisuke Yamaguchi, Architectural Design Division, Kajima Corporation, Tokyo, Japan, kyama@kajima.com

[5] Jun Kubota, Kajima Technical Research Institute, Kajima Corporation, Tokyo, Japan, jkubota@kajima.com

https://doi.org/10.52202/080513-0104

bending moments are transferred by the GIR, and shear forces are transferred by dowels made of perforated steel plates for beams and short round-shape steel tubes for columns considering ease of construction. The performance of the proposed joint was evaluated through full-scale frame experiments. The experiments mainly examined the stiffness and strength of the joint, the strength of the reinforced concrete part, and the stiffness of the dowel. We also examined whether the experimental results could be evaluated using existing evaluation formulas.

2 – STRUCTURAL TEST OUTLINE

An experimental investigation involving a cruciform frame was carried out to assess the structural performance of the proposed beam-column joint. The test specimens are detailed in Table 1. The configurations of the test specimens are shown in Figure 2. Three test specimens of the cruciform full-scale frame were employed. The experimental parameters under consideration were the failure mode, with the aim of understanding the structural performance (e.g., strength, stiffness, level of destruction) of the beam-column joint under different failure scenarios: beam bending, column bending, and panel shear failures. The beams and columns were constructed from laminated timber. The beams were fabricated from larch E120-F330, while the columns were composed of either cedar E65-F255 or larch E105-F345[4]. Specimen No.1 only had steel plate dowels at the beam-to-joint connections which were bonded using the same adhesive as utilized in the GIR joint. In contrast, Specimens No.2 and No.3 featured dowel connections in both the columns and beams. The beams were connected to a steel bracket using dowels and drift pins. The columns were connected to steel pipe dowels. Each connection was designed to transfer shear through the beam-column joint concrete. The beam shear connections for No. 2 and No. 3 were joined on the outside of the reinforcement, resulting in thicker cover concrete.

Test specimens were manufactured following the fabrication process shown in Figure 3. Figure 3 (a) shows the glue injection of the beam for No.1. The laminated timber that comprises the column and beam components was produced by drilling or employing an NC processing machine to create the necessary holes and slits for the insertion of rebar and steel frames. The GIR joint utilized a two-component reactive curing epoxy resin adhesive. For the GIR connections, rebars were inserted into the drilled holes in the column and beam members, with epoxy resin adhesive injected through an opening on the side of the member using a nozzle. The anchorage length of the rebar was designed to ensure that the adhesion stress at the interface between the epoxy and the wood was approximately 3 N/mm². Figure 3 (b) shows setting the steel connection at the beam end for No.3. Following the injection of the epoxy, shear resistance metal fittings were positioned in their designated locations and secured using drift pins. Shear reinforcement comprised 10 ϕ deformed bars, with nine pieces arranged within the joint. Figure 3 (c) shows mortar injection at the mechanical joint in the centre of the rebars. The rebar was split at the joint's centre and connected with a mortar-filled mechanical joint following the arrangement of the reinforcement. The shear reinforcement was configured in a U-shape and integrated with a wedge-inserted mechanical joint (OS Hoop Clip Method) after the reinforcement was set in place. Subsequently, the column and beam members were assembled, with shear reinforcement integrated using a wedge insertion type mechanical joint and a mortar-filled mechanical joint. Finally, the beam-column joint concrete was cast, resulting in the integration of the column and beam members. Figure 3 (d) shows the concrete being cast at the column and beam intersection.

Table 1: Specimen

ID			No.1	No.2	No.3
Destruction Type			Beam bending	Column bending	Panel shear
Scale			80%	100%	100%
Beam	Span	[mm]	6000	6000	6000
	Section	[mm×mm]	240 × 690	300 × 870	300 × 870
	Material		Larch	Larch	Larch
	Grade[4]		E120-F330	E120-F330	E120-F330
	Number of rebars		8	12	12
	Rebar diameter	[mm]	16	19	19
	Standard yield point of rebars	[N/mm2]	345	345	490
	Reinforcement ratio	[%]	0.62	0.81	0.81
	GIR fixation length	[mm]	500	500	600
Column	Span	[mm]	3180	3180	3180
	Section	[mm×mm]	520 × 520	420 × 420	520 × 520
	Material		Cedar	Cedar	Larch
	Grade[4]		E65-F255	E65-F255	E105-F345
	Number of rebars		8	8	10
	Rebar diameter	[mm]	19	22	22
	Standard yield point of rebars	[N/mm2]	345	345	390
	Reinforcement ratio	[%]	0.38	0.81	0.76
	GIR fixation length	[mm]	500	500	600
	Axial force	[kN]	600	400	1000
	Axial pressure ratio		0.11	0.11	0.13
Concrete	Fc	[N/mm2]	36	24	24

https://doi.org/10.52202/080513-0104

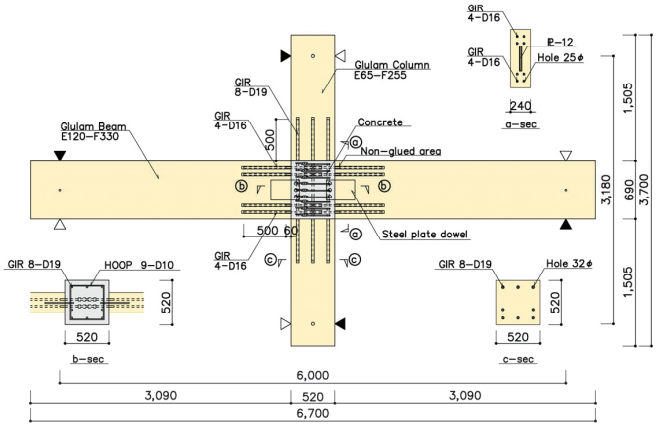

No.1 Beam Bending Failure

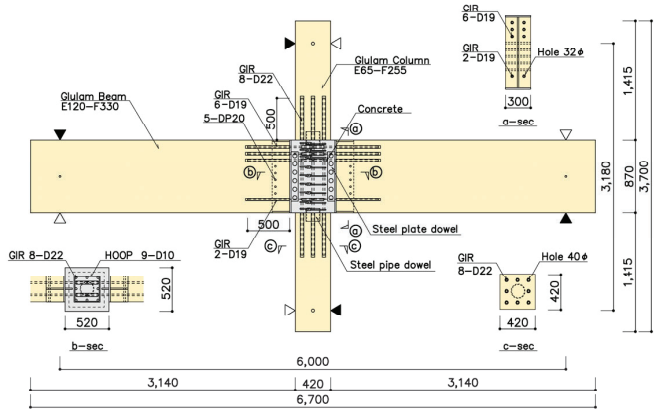

No.2 Column Bending Failure

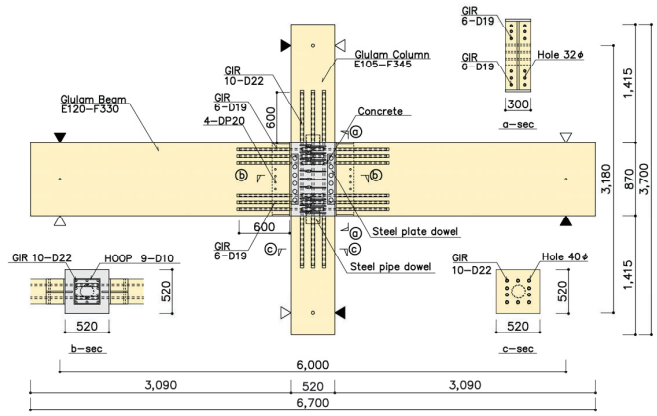

No.3 Panel Shear Failure

Figure 2: Specimen plan

(a) Glue injection at beam end

(b) Setting steel connection at beam end

(c) Mortar injection at mechanical joint in the centre of rebars

(d) Casting concrete at column and beam intersection

(e) Finished product after formwork removal

Figure 3: Specimen fabrication

https://doi.org/10.52202/080513-0104

The loading apparatus is shown in Figure 4. The loading methodology was designed with reference to the standard for timber structures in Japan [5]. The loading process involved simply supporting both ends of the column, to which a specified axial load was applied, and subsequently subjecting the beams to cyclic loading using a 500-kN push-pull jack positioned at the beam's end, with alternating positive and negative incremental displacements. The loading history proceeded as follows: under beam end displacement control, the inter-story drift angle R=δ/L (where δ represents the vertical displacement difference between the left and right ends of the beam, and L denotes the distance between the left and right loading points on the beam) was set to 1/800 rad. (hereafter, "rad." will be omitted), followed by 1/450, 1/300, 1/200, 1/150, 1/100, 1/75, and 1/50, each repeated three times, concluding the experiment at 1/30. During the loading process, a reaction force was applied to the column using a reaction jack to ensure that the test specimen remained stationary. Out-of-plane restraint jigs were utilized at the ends of the beams to prevent any out-of-plane deformation.

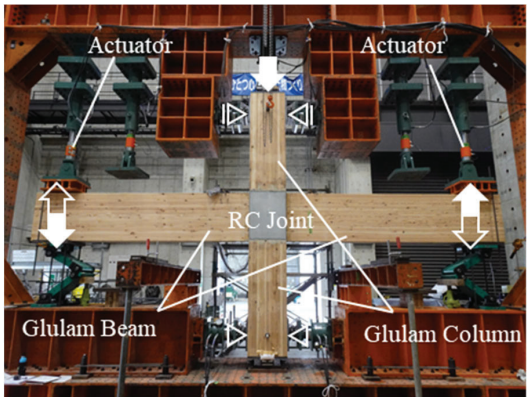

Figure 4: Experimental setup

3 – RESULTS

The relationship between average beam shear force and story drift angle observed under cyclic loading is shown in Figure 5. The calculated initial stiffness and calculated ultimate strength are also shown by red lines. The calculation method will be described the following section. Figure 6 shows photographs of the damage sustained at story drift angles of 1/100 rad. and after the test. Cracks that appeared on the surface of the reinforced concrete during the experiment were traced with a pen to make them easier to see. The subsequent sections detail the experimental progression and destruction characteristics of each specimen.

(1) No.1 Beam Bending Failure

Elastic behaviour was observed until the rebar of the beam yielded at approximately 1/200 rad. Beyond this point, gaps formed at the beam-to-joint due to the rotation and embedment of the beam, expanding to a maximum width of 13 mm. The width of the cracks in the reinforced concrete remained minimal, indicating that their impact on the frame was negligible. No significant damage was detected in the beam-column components throughout the test, and the beam ultimately failed in bending as anticipated. Furthermore, the load corresponding to the strength could be predicted by calculation.

(2) No.2 Column Bending Failure

The yielding of the rebar in the column and the emergence of shear cracks in the reinforced concrete were observed at approximately 1/100 to 1/75 rad., followed by the yielding of the rebar in the beam. Subsequently, a reduction in stiffness was noted, with the maximum strength attained at a peak drift of 1/50 rad. Notably, even after reaching the maximum strength, there was no significant reduction in load, and the experiment concluded at a cycle of ±1/30 rad. This indicates that the frame exhibits stable hysteretic characteristics without considerable load reduction even within the large deformation range. Post-experiment, gaps in the column joint surface and cracks in the reinforced concrete could be observed; however, no substantial damage was detected within the beam-column member itself. The bending yield of the column was verified under a load that corresponded to the strength anticipated in the design, demonstrating the stiffness and strength required for practical application. Furthermore, at 1/200 rad. (the limited maximum drift during level 1 earthquakes in Japan [4]), the cracks in the reinforced concrete did not widen and gaps at the column end were not observed, suggesting that the degree of damage to the joints was acceptable for the level of the present design.

(3) No.3 Panel Shear Failure

Shear cracks manifested in the joint concrete at approximately 1/150 rad, leading to a decline in stiffness, which peaked at a strength corresponding to 1/50 rad. The maximum strength was attained at this peak displacement. At 1/30 rad, the crack widened to 12 mm, culminating in significant spalling of the concrete in the cover section. No notable damage was observed in the beam-column member, and yielding of the primary reinforcement in the columns or beams was not detected. Moreover, no gaps were identified on the surface of the beam-column joint, with the predominant failure mode being shear failure of the reinforced concrete, as initially hypothesized. However, the panel did not achieve the shear strength anticipated during the design phase [7]. This is attributed to the cover concrete section, which was not reinforced by reinforcements in the design details of this joint, thus failing to contribute to the overall shear strength. Therefore, the calculated strength shown in the figure does not include the contribution of the cover concrete. The calculation method will be described the following section.

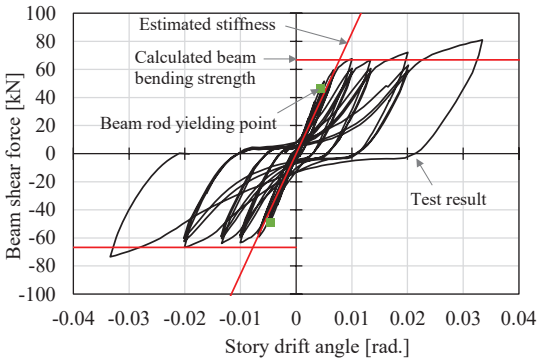

No.1 Beam Bending Failure

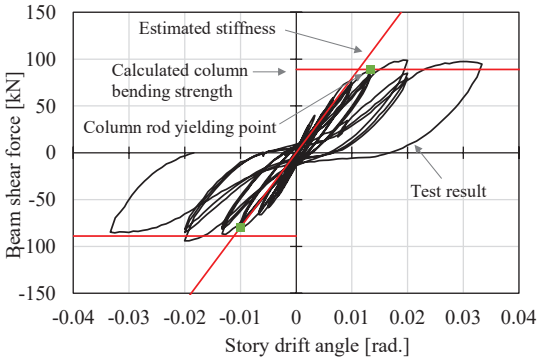

No. 2 Column Bending Failure

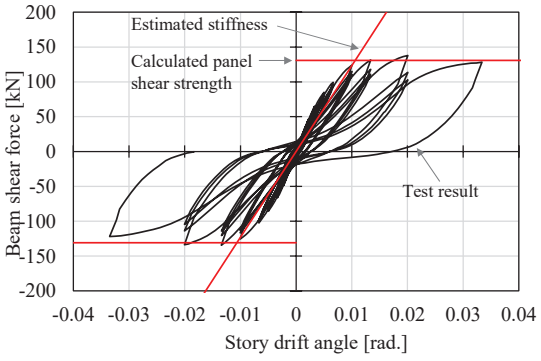

No. 3 Panel Shear Failure

Figure 5: Relationship between beam shear force and drift angle.

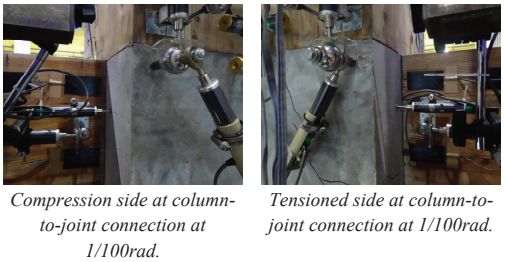

Compression side at column-to-joint connection at 1/100rad. *Tensioned side at column-to-joint connection at 1/100rad.*

Concrete joint at 1/100rad. *Specimen after the test*

No.1 Beam Bending Failure

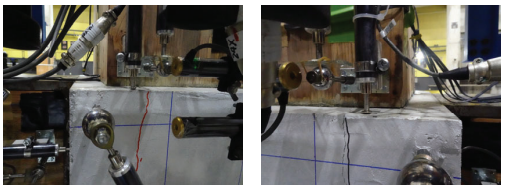

Compression side at column-to-joint connection at 1/100rad. *Tensioned side at column-to-joint connection at 1/100rad.*

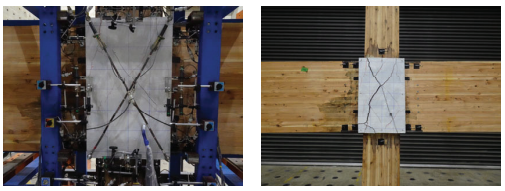

Concrete joint at 1/100rad. *Specimen after the test*

No. 2 Column Bending Failure

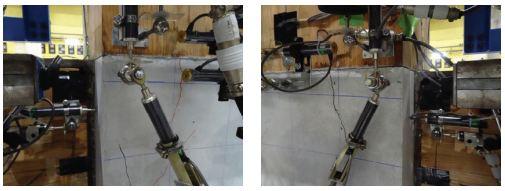

Compression side at column-to-joint connection at 1/100rad. *Tensioned side at column-to-joint connection at 1/100rad.*

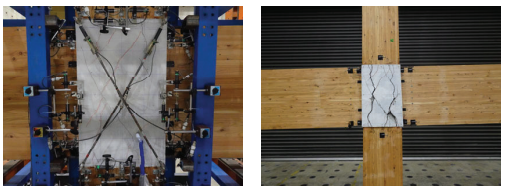

Concrete joint at 1/100rad. *Specimen after the test*

No. 3 Panel Shear Failure

Figure 6: Photo of test specimen during loading at 1/100rad. and after the test.

https://doi.org/10.52202/080513-0104

Figure 7 shows the relationship between the slip displacement of the timber-concrete in the 1st cycle and the story drift angle for each specimen. In all test specimens, the displacement remained below 1 mm up to 1/100 rad, which is the range in which the ultimate strength is reached, demonstrating the effectiveness of the shear resistance joints. The reason why the column slip displacement relative to the beam is small is that the frictional force generated by the axial force applied to the column resists the slipping deformation. For No.1, although no shear joint is provided on the column, it can be assumed that friction resistance and the relatively small load result in sufficient resistance.

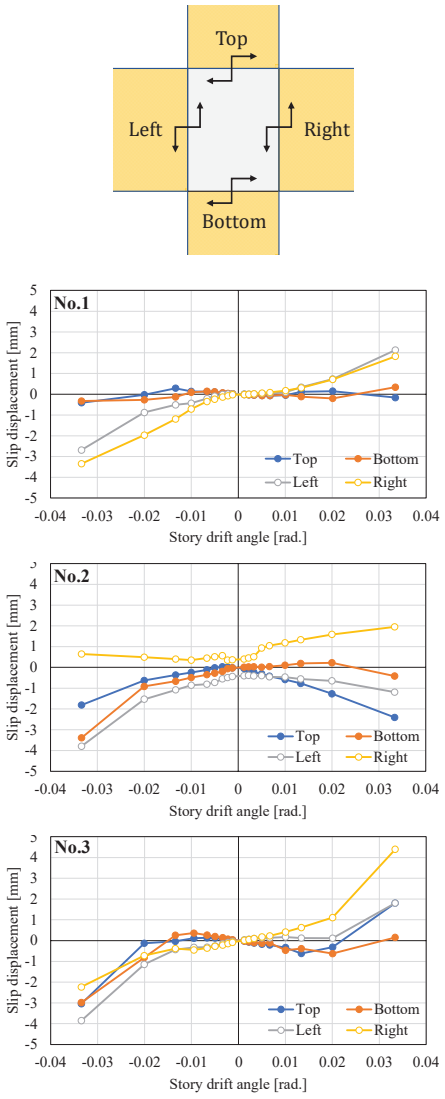

Figure 7: Slip displacement between timber and concrete.

4 – EVALUATION FORMULAS

The stiffness of wooden rigid frames is significantly impacted by rotational deformation at the joints; thus, it is imperative to assess the rotational stiffness at the ends of columns and beams. We examine the evaluation formulas for stiffness and strength derived from experimental data.

(1) Calculation of Rotational Stiffness

We propose an evaluation formula for the rotational stiffness. The proposed mechanical model is shown in Figure 8. The moment generated at the ends is countered by the tensile force of the rebars and the compressive force at the edge, as described by equation (1). In this context, the distance to the centroid of stress, denoted as (j), is determined using equation (2). The combined tensile force exerted by the rebars at an arbitrary rotation angle (θ) is computed through equation (3). Furthermore, the end of the wood is postulated to exhibit a triangular displacement and embedment, with the combined compressive force calculated using equation (4). In this case, the compressive edge strain (ε_w) is derived from equation (5), under the assumption that the area where the strain in the fibre direction occurs is (x_n/2). The position of the neutral axis (x_n) is determined via equation (7), based on the equilibrium between tensile and compressive forces. By rearranging the equations, the moment can be articulated as a linear function of (θ) (equation (8)), allowing for the calculation of rotational stiffness ($K_\theta = M/\theta$) as per equation (9).

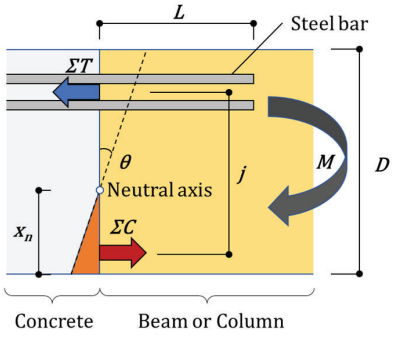

Figure 8 Mechanical model

$$M = \Sigma C j \quad (1)$$

$$j = D - \frac{1}{3}x_n - \frac{\sum d_n T_n}{\sum T_n} \quad (2)$$

$$\Sigma T = \Sigma(a_t E_s \varepsilon_n) = \frac{\Sigma[a_t E_s (D - x_n - d_n)\theta]}{L} \quad (3)$$

$$\Sigma C = \frac{1}{2} B x_n E_w \varepsilon_w = B x_n E_w \theta \quad (4)$$

$$\varepsilon_w = \frac{x_n \theta}{x_n/2} = 2\theta \quad (5)$$

$$\Sigma T = \Sigma C \quad (6)$$

$$x_n = \Sigma[a_t(D - d_n)]/(\frac{BL_e E_w}{E_s} + \Sigma a_t) \quad (7)$$

$$M = B x_n E_w \theta j \quad (8)$$

$$K_\theta = M/\theta = B x_n E_w j \quad (9)$$

https://doi.org/10.52202/080513-0104

ΣC: Compressive force at the end of the wood
ΣT: Tensile force of the rebar
D: Beam depth
B: Beam width
x_n: Distance from the compression edge to the neutral axis
d_n: Distance from the top of the beam to the n^{th} rebar
T_n: Tensile force of the n^{th} rebar from the top of the beam
a_t: Rebar cross-sectional area
E_s: Young's modulus of the rebar
E_w: Young's modulus in the direction of the grain of the wood
ε_n: Tensile strain of the rebar
ε_w: Compressive edge strain of the laminated timber
L: Anchorage length of the rebar

(2) Calculation of Ultimate Bending Strength

The ultimate bending strength of the columns and beams was determined by employing the formula for the ultimate bending strength of reinforced concrete, specifically the method based on stress blocks, hereafter referred to as the ACI formula, as proposed by the American Concrete Institute (ACI) [6]. The compressive strength of wood was derived from the results of material tests.

(3) Calculation of Panel Shear Strength

The shear fracture strength of the panel was determined using formula (10), which references the strength evaluation formula for reinforced concrete, specifically the design guidelines in Japan [7]. In this instance, the panel's configuration features a substantial area lacking reinforcements, resulting in considerable damage to the cover concrete; thus, it is inferred that the cover does not contribute to the shear strength. In the previous formula, Effective width is the average of the width of the column and the beam, considering this destructive condition, and the strut effective width developed within the panel was calculated as the shear reinforcement width.

$$Q_{JU} = \varphi F_j b_j{}' D_j \quad (10)$$

ϕ: Correction coefficient depending on the presence or absence of orthogonal beams (without orthogonal beams: 0.85)
F_j: Standard value of shear strength of the joint
$b_j{}'$: Effective width (= shear reinforcement width)
D_j: Column height

(4) Comparison of Experiments and Calculations

Table 2 presents the comparison of the experiments and calculations. Figure 9 shows how the rotation angle is calculated. The rotational stiffness was recorded at 1/200 rad, which was calculated by dividing the displacement difference of the displacement gauges installed at the ends of the beam by the distance between the displacement gauges. We established that the calculated results for both beams and columns across all test specimens accurately correspond to the initial stiffness associated with rotational deformation. In this analysis, the rotational stiffness of the columns was computed without accounting for the axial force, and the resultant stiffness closely aligned with the experimental findings, suggesting that axial force has a negligible effect on rotational stiffness. Conversely, the validity of considering the length of the reinforcing bars

Table 3: Comparison of experiments and calculations

			Rotational Stiffness		Maximum Strength
			Beam	Column	
			$K_{\theta b}$ (kNm/rad.)	$K_{\theta c}$ (kNm/rad.)	Q_{max} (kN)
No.1	**exp**	+	80739	115043	81.0
		-	81731	119440	73.6
		Ave.	**81235**	**117241**	**77.3**
	cal		72018	100513	66.8
	exp/cal		1.13	1.17	1.16
No.2	**exp**	+	71374	69208	99.0
		-	266098	65151	94.1
		Ave.	**168736**	**67179**	**96.5**
	cal		176054	53430	89.0
	exp/cal		0.96	1.26	1.08
No.3	**exp**	+	187904	116210	137.9
		-	212160	122775	134.4
		Ave.	**200032**	**119493**	**136.2**
	cal		205670	95038	131.0
	exp/cal		0.97	1.26	1.04

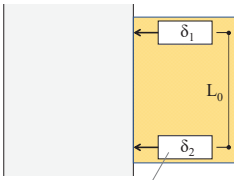

Figure 9: Calculating the rotation angle.

https://doi.org/10.52202/080513-0104

when calculating their tensile stiffness, as well as the assumption regarding the strain area (x_n /2) at the compression edge, has yet to be substantiated. Therefore, future studies should validate these aspects in greater detail in through elemental experiments and analyses.

Next, we will discuss the ultimate bending strength. Table 2 compares the experiments and calculations for the maximum bending strength of No.1 and No.2, which indicate that the evaluation was appropriate. Conversely, the assumptions regarding the compressive edge strain and the width of the compression area within the ACI formula may not be entirely valid due to the differing stress-strain relationships between concrete and wood; thus, verifying the adequacy of these assumptions remains a task for future investigation.

Finally, we will discuss the panel shear strength. The comparison of experiments and calculations are shown in Table 2 for the maximum strength of No.3. The calculated values accurately represent the experimental values. Therefore, the formula we use can adequately evaluate the experimental results.

5 – CONCLUSION

In the context of decarbonization within the construction industry, the demand for timber structure buildings is on the rise. Typically, the ends of beams and columns have been designed as pin or semi-rigid connections, resulting in inefficient bending moment transfer due to the limited stiffness of wood in the perpendicular direction to the grain. We proposed hybrid moment connections for timber frames which are made up of timber beams and columns and concrete joints. It reduces the risk of wood embedding, thereby enhancing the stiffness of timber structures and facilitating more rational structural design.

In this study, we fabricated three test specimens and conducted experiments with different failure modes to verify the performance of the joints. Through the fabrication of test specimens, we determined that the proposed joint can be constructed without complications and verified that the construction was rational. The full-scale frame experiments demonstrated that the strength of all test specimens reached a ceiling at approximately 1/100 rad. and exhibited the anticipated failure mode. The specimens possessed stiffness, strength, and ductility such that the load did not decrease up to 1/30 rad.

Moreover, the iron dowels were determined to worked effective, and there were small slip displacements between timber and concrete joints. Lastly, we established that the performance of the joints, as validated in the experiments, can be assessed with a high degree of accuracy by employing existing evaluation formulas. However, certain assumptions utilized in the calculations necessitate validation through additional experiments in future research endeavours.

6 – REFERENCES

[1] Étienne Gauthier-Turcotte, Sylvain Ménard, and Mathieu Fiset. “Strength and Behavior of Spruce Pine Glulam Timber Moment Connections Using Glued-In Steel Rods.” In: Journal of Structural Engineering, 2022, 04022192

[2] Gilbert, C. F., and Erochko, J. (2019). "Development and testing of hybrid timber-steel braced frames." Engineering Structures, 198, 109495.

[3] Stepinac, M., Rajcic, V., Hunger, F., van de Kuilen, J.-W., Tomasi, R., and Serrano, E. (2013). "Comparison of design rules for glued-in rods and design rule proposal for implementation in European standards." Proc., CIB-W18/46-7-10, International Council for Research and Innovation in Building and Construction, Working Commission W18 - Timber Structures, Vancouver, Canada.

[4] Architectural Institute of Japan: AIJ Standard for Structural Design of Timber Structures, Tokyo, Japan, Maruzen, 2006. (in Japanese)

[5] Japan Housing and Wood Technology Center: Design and construction manual on timber frame structure version 2016, Tokyo, Japan, 2016. (in Japanese)

[6] American Concrete Institute: ACI 318-05Building Code Requirements for Structural Concrete and Commentary, 2005

[7] Architectural Institute of Japan: AIJ Design Guidelines for Earthquake Resistant Reinforced Concrete Buildings Based on Inelastic Displacement Concept, Tokyo, Japan, Maruzen, 1999. (in Japanese)